Engineering Notes

ENGINEERING NOTES are short manuscripts describing new developments or important results of a preliminary nature. These Notes cannot exceed 6 manuscript pages and 3 figures; a page of text may be substituted for a figure and vice versa. After informal review by the editors, they may be published within a few months of the date of receipt. Style requirements are the same as for regular contributions (see inside back cover).

Model Atmospheres of Mercury

OTHA H. VAUGHAN JR.*
NASA Marshall Space Flight Center, Huntsville, Ala.

THIS Note presents atmospheric models for use in preliminary design studies for a spacecraft to probe the environment of Mercury.[1] Geophysical and astronomical data for Mercury are summarized in Table 1. Mercury is the smallest of the major planets of the solar system. Its orbital eccentricity is greater than that of any other planet in the solar system excluding Pluto. Mercury's orbital path and location with respect to the sun make it difficult to observe, since at its most favorable elongation it recedes only 28° from the sun in the plane of the ecliptic. Several volumes have been written about the techniques of observing and obtaining environmental data for the planets of our solar system (Refs. 2–4 are comprehensive sources).

In 1936, Pettit and Nicholson[3,5] made infrared measurements over a number of phase angles, obtaining a surface temperature at the subsolar point of 610°K. Walker in 1961[6] calculated the mean subsolar temperature to be 621°K and the dark-side temperature to be 28°K by assuming that: 1) the planet did not rotate, 2) the interior was in thermal steady state, 3) the specific rate of radioactive heat production was equal to that of chrondritic meteorites (1.33 cal $deg^{-1}cm^{-1}$ m^{-1}), and 4) the planet was at a mean orbital distance. Because of the orbital eccentricities, the subsolar temperature as determined by Pettit[3] can be as high as 688°K at perihelion and 588°K at aphelion by assuming that the subsolar temperature is 613°K when the planet is at its mean distance from the sun.

Evidence for an atmosphere of Mercury has been based mainly on polarization studies,[7,8] spectrographic data,[3,9–12] and thermal data.[13–15] Early polarization studies by Lyot and later by Dollfus[8] provided the first evidence for an atmosphere. Dollfus examined the distribution of polarized light from different parts of the planet. At small phase angles, there appeared to be no difference in polarization for the bright or dark regions. However, as the phase angle increased, the polarization became stronger at the tips than at the center of the crescent. Since the moon does not exhibit this phenomenon, and since the surfaces of Mercury and the moon are considered similar, Dollfus concluded that this excessive polarization was the result of a weak atmosphere.

In 1963 Kozyrev[12,16] obtained 20 spectrograms of the planet and of its near vicinity. For comparison, spectrograms of the sun had been taken at the same position where Mercury would be when the spectrograms of the planet and vicinity were programed to be taken. Analysis of the data revealed some hydrogen lines which seemed to have shifted toward the violet region, whereas other hydrogen lines appeared to have shifted toward the red region of the spectrum. Because the ultraviolet radiation of the sun, in ionizing hydrogen, is not sufficient to produce these effects, the data implied that hydrogen was present as a genuine dense atmosphere rather than an ionosphere. Kozyrev believed that, since Mercury is the nearest planet to the sun, a tenuous hydrogen atmosphere might be maintained by fluxes of protons from the sun. Obscuration of surface features as noted by Antoniadi and Futschek and Severinski (cited by Sandner[17]), who claimed to have detected an aureole surrounding the planet, are also evidence for an atmosphere. According to Spinrad and Hodge,[10,11] the spectrographic, polarization, and radio observations lead to the conclusion that the planet does have a tenuous atmosphere and that it may be time variable. Field,[13] in his analysis of microwave emission (3-cm wavelength) data obtained by Howard, Barrett, and Haddock,[18] observed a systematic tendency of the brightness temperature data to lie above the theoretical curve of brightness temperature with respect to phase, assuming a back-side temperature of 0°K. He suggested that an atmosphere is responsible for the transport of heat to the dark side. Barrett,[19] after analysis of data from Ref. 18, postulated that the dark-side temperatures as predicted by Walker[6] were not as low as 28°K but could be close to 270°K.

By means of microwave equipment (1.53-cm wavelength), Welch and Thornton[20] obtained brightness measurements of Jupiter, Saturn, and Mercury in September 1964, while Mercury's average illumination was ~25%. From these data they obtained a mean disk temperature of 465° ± 115°K for Mercury. By assuming a subsolar temperature of 620°K and a pole-darkening proportional to $\cos^{1/2}\theta$, they postulated that the contribution of temperature from the unilluminated part of the disk was ~100°K. Also, by assuming that the properties of the surface materials of Mercury are similar to those of the moon (as indicated by polarization studies), they theorized that the large dark-side contribution to the disk temperature is a result of internal radioactive heat sources.

Table 1 Planetary geophysical and astronomical data for Mercury[5,7,27,29–32]

Mean distance (Earth = 1 a.u.)	0.387099 a.u.
Perihelion	45,980,000 km
Aphelion	69,780,000 km
Orbital velocity	47.87 km/sec
Sidereal period	87.969 days
Orbital inclination to ecliptic	7.00399°
Orbital eccentricity	0.205627
Equatorial radius	2,422 km
Flattening	...
Mass of planet (Earth = 1)	0.056
Mean density	5.13 g/cm³
Velocity of escape	4.2 km/sec
Rotation period	58.4 ± 0.4 days
Inclination of equator to orbit	0°
Gravitational parameter	21,685.53 km³/sec²
Visual albedo	0.056
Mass of sun (Mercury = 1)	6,120,000
Theoretical temperature	
Spherical blackbody (rapidly rotating)	441°K
Hemispherical blackbody (slowly rotating)	525°K
Subsolar blackbody (mean measured value)	624°K

Presented as Paper 69-54 at the AIAA 7th Aerospace Sciences Meeting, New York, January 20–22, 1969; submitted February 24, 1969; revision received June 6, 1969.

* Scientific Assistant—Environment Design Criteria, Aerospace Environment Division, Aero-Astrodynamics Laboratory. Member AIAA.

Table 2 Model atmospheres of Mercury: sunlit side; surface temperature = 520°K

a) Minimum density: 100% CO_2; mesopause at 145 km

h, km	T, °K	p, mb	ρ, gm/cm³	a, m/sec	ℳ	β, km	n, cm⁻³	ℓ, m	μ, kg/m-sec
0.0	520.00	1.000×10^{0}	1.018×10^{-6}	370.90	44.0	34.03	1.393×10^{16}	1.213×10^{-3}	2.742×10^{-5}
5.0	498.79	8.259×10^{-1}	8.762×10^{-7}	363.26	44.0	32.78	1.200×10^{16}	1.409×10^{-3}	2.666×10^{-5}
10.0	477.67	6.770×10^{-1}	7.500×10^{-7}	355.48	44.0	31.53	1.027×10^{16}	1.646×10^{-3}	2.588×10^{-5}
15.0	456.64	5.505×10^{-1}	6.379×10^{-7}	347.57	44.0	30.26	8.734×10^{15}	1.935×10^{-3}	2.509×10^{-5}
20.0	435.70	4.436×10^{-1}	5.388×10^{-7}	339.50	44.0	27.52	7.377×10^{15}	2.291×10^{-3}	2.428×10^{-5}
25.0	424.17	3.549×10^{-1}	4.428×10^{-7}	334.98	44.0	25.11	6.063×10^{15}	2.787×10^{-3}	2.383×10^{-5}
50.0	368.83	1.073×10^{-1}	1.540×10^{-7}	312.37	44.0	22.28	2.109×10^{15}	8.014×10^{-3}	2.155×10^{-5}
75.0	314.60	2.753×10^{-2}	4.632×10^{-8}	288.49	44.0	19.39	6.341×10^{14}	2.665×10^{-2}	1.914×10^{-5}
100.0	261.44	5.652×10^{-3}	1.144×10^{-8}	262.99	44.0	16.44	1.566×10^{14}	1.079×10^{-1}	1.658×10^{-5}
125.0	222.29	8.647×10^{-4}	2.016×10^{-9}	245.03	43.1	12.66	2.760×10^{13}	5.996×10^{-1}	1.478×10^{-5}
150.0	213.45	1.296×10^{-4}	2.932×10^{-10}	248.76	40.2	13.28	4.014×10^{12}	3.842×10^{0}	1.515×10^{-5}
175.0	210.00	2.151×10^{-5}	4.642×10^{-11}	254.71	37.7	13.97	6.355×10^{11}	2.277×10^{1}	1.574×10^{-5}
200.0	210.00	4.066×10^{-6}	8.272×10^{-12}	262.31	35.5	15.05	1.133×10^{11}	1.205×10^{2}	1.651×10^{-5}
300.0	373.99	4.986×10^{-8}	4.522×10^{-14}	392.91	28.2	29.31	6.191×10^{8}	1.749×10^{4}	2.962×10^{-5}
400.0	561.09	7.877×10^{-9}	3.644×10^{-15}	550.13	21.6	53.34	4.988×10^{7}	1.661×10^{5}	4.497×10^{-5}
500.0	735.38	3.161×10^{-9}	7.968×10^{-16}	745.18	15.4	79.72	1.091×10^{7}	5.427×10^{5}	6.346×10^{-5}
600.0	898.14	2.000×10^{-9}	2.587×10^{-16}	1040.44	9.7	94.51	3.542×10^{6}	1.047×10^{6}	9.082×10^{-5}
700.0	960.07	1.577×10^{-9}	1.496×10^{-16}	1215.06	7.6	320.47	2.048×10^{6}	1.420×10^{6}	1.068×10^{-4}
800.0	980.48	1.299×10^{-9}	1.113×10^{-16}	1278.12	7.0	357.46	1.524×10^{6}	1.761×10^{6}	1.126×10^{-4}
900.0	999.66	1.101×10^{-9}	8.532×10^{-17}	1344.37	6.4	395.08	1.168×10^{6}	2.117×10^{6}	1.186×10^{-4}
1000.0	1017.72	9.572×10^{-10}	6.699×10^{-17}	1414.33	5.9	432.65	9.172×10^{5}	2.480×10^{6}	1.250×10^{-4}

b) Mean density: 50% CO_2, 50% Ar; mesopause at 200 km

h, km	T, °K	p, mb	ρ, gm/cm³	a, m/sec	ℳ	β, km	n, cm⁻³	ℓ, m	μ, kg/m-sec
0.0	520.00	5.000×10^{0}	4.857×10^{-6}	379.63	42.0	39.01	6.966×10^{16}	2.426×10^{-5}	2.742×10^{-5}
5.0	493.49	4.161×10^{0}	4.260×10^{-6}	369.82	42.0	37.18	6.109×10^{16}	2.766×10^{-5}	2.647×10^{-5}
10.0	467.09	3.431×10^{0}	3.711×10^{-6}	359.80	42.0	35.34	5.322×10^{16}	3.175×10^{-5}	2.549×10^{-5}
15.0	440.80	2.800×10^{0}	3.209×10^{-6}	349.52	42.0	33.49	4.602×10^{16}	3.672×10^{-5}	2.448×10^{-5}
20.0	429.68	2.265×10^{0}	2.663×10^{-6}	345.09	42.0	25.32	3.820×10^{16}	4.424×10^{-5}	2.404×10^{-5}
25.0	422.87	1.828×10^{0}	2.184×10^{-6}	342.34	42.0	25.02	3.132×10^{16}	5.396×10^{-5}	2.378×10^{-5}
50.0	389.24	6.003×10^{-1}	7.790×10^{-7}	328.45	42.0	23.50	1.117×10^{16}	1.512×10^{-4}	2.241×10^{-5}
75.0	356.29	1.828×10^{-1}	2.592×10^{-7}	314.24	42.0	21.95	3.718×10^{15}	4.545×10^{-4}	2.101×10^{-5}
100.0	323.99	5.098×10^{-2}	7.948×10^{-8}	299.65	42.0	20.36	1.140×10^{15}	1.482×10^{-3}	1.957×10^{-5}
125.0	292.32	1.280×10^{-2}	2.211×10^{-8}	284.63	42.0	18.74	3.172×10^{14}	5.328×10^{-3}	1.809×10^{-5}
150.0	261.27	2.829×10^{-3}	5.470×10^{-9}	269.09	42.0	17.08	7.846×10^{13}	2.154×10^{-2}	1.657×10^{-5}
175.0	230.81	5.350×10^{-4}	1.171×10^{-9}	252.92	42.0	14.85	1.679×10^{13}	1.006×10^{-1}	1.498×10^{-5}
200.0	209.88	9.107×10^{-5}	2.069×10^{-10}	248.23	39.6	14.31	2.968×10^{12}	5.375×10^{-1}	1.453×10^{-5}
300.0	245.81	1.452×10^{-7}	2.225×10^{-13}	302.32	31.3	17.56	3.191×10^{9}	3.947×10^{2}	1.984×10^{-5}
400.0	474.91	9.581×10^{-9}	5.743×10^{-15}	483.27	23.7	41.56	8.237×10^{7}	1.156×10^{4}	3.742×10^{-5}
500.0	688.33	3.138×10^{-9}	9.077×10^{-16}	695.67	16.6	69.06	1.302×10^{7}	5.117×10^{4}	5.730×10^{-5}
600.0	887.62	1.897×10^{-9}	2.548×10^{-16}	1020.94	9.9	84.51	3.655×10^{6}	1.091×10^{5}	8.686×10^{-5}
700.0	960.07	1.493×10^{-9}	1.416×10^{-16}	1215.06	7.6	320.47	2.031×10^{6}	1.499×10^{5}	1.043×10^{-4}
800.0	980.48	1.230×10^{-9}	1.054×10^{-16}	1278.12	7.0	357.46	1.512×10^{6}	1.859×10^{5}	1.099×10^{-4}
900.0	999.66	1.043×10^{-9}	8.079×10^{-17}	1344.37	6.4	395.08	1.159×10^{6}	2.236×10^{5}	1.158×10^{-4}
1000.0	1017.72	9.064×10^{-10}	6.344×10^{-17}	1414.33	5.9	432.65	9.098×10^{5}	2.619×10^{5}	1.220×10^{-4}

c) Maximum density: 60% CO_2, 25% Ne, 15% N_2; mesopause at 280 km

h, km	T, °K	p, mb	ρ, gm/cm³	a, m/sec	ℳ	β, km	n, cm⁻³	ℓ, m	μ, kg/m-sec
0.0	520.00	5.000×10^{0}	4.117×10^{-6}	412.34	35.6	43.56	6.966×10^{16}	2.426×10^{-4}	2.742×10^{-5}
5.0	500.72	4.284×10^{0}	3.664×10^{-6}	404.62	35.6	42.12	6.199×10^{16}	2.726×10^{-4}	2.673×10^{-5}
10.0	481.52	3.651×10^{0}	3.247×10^{-6}	396.79	35.6	40.68	5.494×10^{16}	3.076×10^{-4}	2.603×10^{-5}
15.0	462.40	3.094×10^{0}	2.865×10^{-6}	388.83	35.6	39.22	4.847×10^{16}	3.486×10^{-4}	2.531×10^{-5}
20.0	443.36	2.605×10^{0}	2.516×10^{-6}	380.74	35.6	37.76	4.257×10^{16}	3.970×10^{-4}	2.458×10^{-5}
25.0	431.62	2.180×10^{0}	2.163×10^{-6}	375.67	35.6	30.25	3.660×10^{16}	4.617×10^{-4}	2.412×10^{-5}
50.0	401.71	8.692×10^{-1}	9.264×10^{-7}	362.42	35.6	28.73	1.568×10^{16}	1.078×10^{-3}	2.292×10^{-5}
75.0	372.41	3.294×10^{-1}	3.787×10^{-7}	348.95	35.6	27.17	6.408×10^{15}	2.637×10^{-3}	2.170×10^{-5}
100.0	343.69	1.178×10^{-1}	1.468×10^{-7}	335.23	35.6	25.58	2.484×10^{15}	6.804×10^{-3}	2.046×10^{-5}
125.0	315.53	3.941×10^{-2}	5.348×10^{-8}	321.20	35.6	23.96	9.050×10^{14}	1.867×10^{-2}	1.919×10^{-5}
150.0	287.92	1.220×10^{-2}	1.814×10^{-8}	306.83	35.6	22.29	3.069×10^{14}	5.507×10^{-2}	1.788×10^{-5}
175.0	260.84	3.441×10^{-3}	5.648×10^{-9}	292.04	35.6	20.59	9.558×10^{13}	1.768×10^{-1}	1.655×10^{-5}
200.0	244.10	8.883×10^{-4}	1.540×10^{-9}	284.21	35.2	18.60	2.605×10^{13}	6.409×10^{-1}	1.584×10^{-5}
300.0	206.05	3.683×10^{-6}	6.973×10^{-12}	271.93	32.4	18.40	1.180×10^{11}	1.305×10^{2}	1.473×10^{-5}
400.0	361.30	6.738×10^{-8}	5.134×10^{-14}	428.67	22.9	31.89	8.686×10^{8}	1.251×10^{4}	2.889×10^{-5}
500.0	626.30	1.839×10^{-8}	5.696×10^{-15}	672.32	16.1	62.55	9.637×10^{7}	7.944×10^{4}	5.020×10^{-5}
600.0	873.75	1.092×10^{-8}	1.475×10^{-15}	1017.85	9.8	82.27	2.496×10^{7}	1.867×10^{5}	7.931×10^{-5}
700.0	952.89	8.586×10^{-9}	8.203×10^{-16}	1210.51	7.6	329.74	1.388×10^{7}	2.589×10^{5}	9.526×10^{-5}
800.0	963.58	7.054×10^{-9}	6.151×10^{-16}	1267.07	7.0	365.68	1.041×10^{7}	3.186×10^{5}	9.992×10^{-5}
900.0	973.63	5.959×10^{-9}	4.740×10^{-16}	1326.76	6.4	402.30	8.020×10^{6}	3.811×10^{5}	1.048×10^{-4}
1000.0	983.09	5.157×10^{-9}	3.736×10^{-16}	1390.06	5.9	438.96	6.322×10^{6}	4.447×10^{5}	1.100×10^{-4}

Additional information still was required to determine whether Mercury has an atmosphere. Before 1965, Mercury was considered to be in synchronous rotation, and the high back-side temperature could be explained if there was an atmosphere to transport the heat to the dark side. Recent radar probe measurements by Pettengill and his associates[21,22] at Arecibo, Puerto Rico, during the 1965 inferior conjunction of Mercury, indicated that the rotational period was different from the orbital period. The rotation of the planet is now considered to be direct with a sidereal period of 59 ± 5 days. Although the direction of the pole is not well determined from these limited data, Pettengill and Dyce[21] agree that it is approximately normal to the planetary orbit. Analysis of these data by Peale and Gold[23] indicated that 1) the rotation rate was between 56.6 and 88 days, 2) Mercury has little permanent rigidity, and 3) the nonsynchronous rotation may be ex-

Table 3 Model atmospheres of Mercury: dark side; surface temperature = 270°K

h, km	T, °K	p, mb	ρ, gm/cm³	a, m/sec	$\mathfrak{M}$	β, km	n, cm⁻³	ℓ, m	μ, kg/m-sec
a) Minimum density: 100% CO_2; mesopause at 145 km									
0.0	270.00	5.000×10^{-1}	9.800×10^{-7}	267.26	44.0	14.19	1.342×10^{16}	1.259×10^{-3}	1.700×10^{-5}
5.0	267.51	3.479×10^{-1}	6.883×10^{-7}	266.02	44.0	14.12	9.424×10^{15}	1.793×10^{-3}	1.688×10^{-5}
10.0	265.02	2.417×10^{-1}	4.826×10^{-7}	264.78	44.0	14.04	6.607×10^{15}	2.558×10^{-3}	1.676×10^{-5}
15.0	262.55	1.675×10^{-1}	3.377×10^{-7}	263.55	44.0	13.97	4.623×10^{15}	3.655×10^{-3}	1.663×10^{-5}
20.0	260.08	1.159×10^{-1}	2.359×10^{-7}	262.31	44.0	13.86	3.229×10^{15}	5.233×10^{-3}	1.651×10^{-5}
25.0	258.20	8.008×10^{-2}	1.641×10^{-7}	261.35	44.0	13.76	2.247×10^{15}	7.520×10^{-3}	1.641×10^{-5}
50.0	248.97	1.238×10^{-2}	2.631×10^{-8}	256.64	44.0	13.55	3.602×10^{14}	4.691×10^{-2}	1.594×10^{-5}
75.0	239.93	1.855×10^{-3}	4.092×10^{-9}	251.94	44.0	13.32	5.602×10^{13}	3.017×10^{-1}	1.547×10^{-5}
100.0	231.07	2.690×10^{-4}	6.160×10^{-10}	247.25	44.0	13.09	8.433×10^{12}	2.004×10^{0}	1.500×10^{-5}
125.0	222.29	3.787×10^{-5}	8.831×10^{-11}	245.03	43.1	12.67	1.209×10^{12}	1.369×10^{1}	1.478×10^{-5}
150.0	213.46	5.677×10^{-6}	1.284×10^{-11}	248.76	40.2	13.28	1.758×10^{11}	8.770×10^{1}	1.515×10^{-5}
175.0	210.00	9.424×10^{-7}	2.034×10^{-12}	254.70	37.7	13.97	2.784×10^{10}	5.197×10^{2}	1.574×10^{-5}
200.0	210.00	1.782×10^{-7}	3.625×10^{-13}	262.31	35.5	15.05	4.963×10^{9}	2.749×10^{3}	1.651×10^{-5}
300.0	373.93	2.185×10^{-9}	1.982×10^{-15}	392.87	28.2	29.31	2.713×10^{7}	3.992×10^{5}	2.961×10^{-5}
400.0	560.99	3.451×10^{-10}	1.597×10^{-16}	550.04	21.6	53.34	2.186×10^{6}	3.791×10^{6}	4.497×10^{-5}
500.0	735.24	1.385×10^{-10}	3.492×10^{-17}	744.99	15.4	79.73	4.781×10^{5}	1.239×10^{7}	6.344×10^{-5}
600.0	897.95	8.761×10^{-11}	1.134×10^{-17}	1039.96	9.7	94.55	1.553×10^{5}	2.391×10^{7}	9.077×10^{-5}
700.0	960.03	6.908×10^{-11}	6.552×10^{-18}	1214.95	7.6	320.56	8.970×10^{4}	3.241×10^{7}	1.068×10^{-4}
800.0	980.43	5.689×10^{-11}	4.877×10^{-18}	1277.98	7.0	357.58	6.676×10^{4}	4.019×10^{7}	1.125×10^{-4}
900.0	999.61	4.824×10^{-11}	3.738×10^{-18}	1344.19	6.4	395.22	5.118×10^{4}	4.833×10^{7}	1.186×10^{-4}
1000.0	1017.66	4.193×10^{-11}	2.935×10^{-18}	1414.08	5.9	432.90	4.019×10^{4}	5.661×10^{7}	1.249×10^{-4}
b) Mean density: 50% CO_2, 50% Ar; mesopause at 200 km									
0.0	270.00	3.000×10^{0}	5.613×10^{-6}	273.55	42.0	14.68	8.050×10^{16}	2.099×10^{-4}	1.700×10^{-5}
5.0	268.75	2.124×10^{0}	3.992×10^{-6}	272.92	42.0	14.67	5.726×10^{16}	2.951×10^{-4}	1.694×10^{-5}
10.0	267.51	1.504×10^{0}	2.839×10^{-6}	272.29	42.0	14.67	4.072×10^{16}	4.149×10^{-4}	1.688×10^{-5}
15.0	266.27	1.064×10^{0}	2.019×10^{-6}	271.66	42.0	14.66	2.896×10^{16}	5.836×10^{-4}	1.682×10^{-5}
20.0	265.09	7.531×10^{-1}	1.435×10^{-6}	271.05	42.0	14.64	2.058×10^{16}	8.210×10^{-4}	1.676×10^{-5}
25.0	263.92	5.329×10^{-1}	1.020×10^{-6}	270.45	42.0	14.64	1.463×10^{16}	1.155×10^{-3}	1.670×10^{-5}
50.0	258.15	9.435×10^{-2}	1.846×10^{-7}	267.48	42.0	14.61	2.648×10^{15}	6.381×10^{-3}	1.641×10^{-5}
75.0	252.49	1.665×10^{-2}	3.331×10^{-8}	264.53	42.0	14.58	4.778×10^{14}	3.537×10^{-2}	1.612×10^{-5}
100.0	246.94	2.927×10^{-3}	5.988×10^{-9}	261.61	42.0	14.55	8.588×10^{13}	1.968×10^{-1}	1.583×10^{-5}
125.0	241.51	5.125×10^{-4}	1.072×10^{-9}	258.71	42.0	14.51	1.537×10^{13}	1.099×10^{0}	1.555×10^{-5}
150.0	236.18	8.930×10^{-5}	1.910×10^{-10}	255.84	42.0	14.47	2.740×10^{12}	6.168×10^{0}	1.527×10^{-5}
175.0	230.95	1.548×10^{-5}	3.387×10^{-11}	253.00	42.0	14.50	4.857×10^{11}	3.479×10^{1}	1.499×10^{-5}
200.0	209.84	2.634×10^{-6}	5.986×10^{-12}	248.20	39.6	14.30	8.586×10^{10}	1.858×10^{2}	1.452×10^{-5}
300.0	245.81	4.201×10^{-9}	6.435×10^{-15}	302.32	31.3	17.56	9.229×10^{7}	1.365×10^{5}	1.984×10^{-5}
400.0	474.91	2.771×10^{-10}	1.661×10^{-16}	483.27	23.7	41.56	2.382×10^{6}	3.997×10^{6}	3.742×10^{-5}
500.0	688.33	9.075×10^{-11}	2.625×10^{-17}	695.67	16.6	69.06	3.765×10^{5}	1.769×10^{7}	5.730×10^{-5}
600.0	887.62	5.487×10^{-11}	7.370×10^{-18}	1020.94	9.9	84.51	1.057×10^{5}	3.773×10^{7}	8.686×10^{-5}
700.0	960.07	4.319×10^{-11}	4.096×10^{-18}	1215.06	7.6	320.47	5.874×10^{4}	5.184×10^{7}	1.043×10^{-4}
800.0	980.48	3.557×10^{-11}	3.048×10^{-18}	1278.12	7.0	357.46	4.372×10^{4}	6.429×10^{7}	1.099×10^{-4}
900.0	999.66	3.016×10^{-11}	2.336×10^{-18}	1344.37	6.4	395.08	3.351×10^{4}	7.730×10^{7}	1.158×10^{-4}
1000.0	1017.72	2.621×10^{-11}	1.835×10^{-18}	1414.33	5.9	432.65	2.631×10^{4}	9.056×10^{7}	1.220×10^{-4}
c) Maximum density: 60% CO_2, 25% Ne, 15% N_2; mesopause at 280 km									
0.0	270.00	3.000×10^{0}	4.757×10^{-6}	297.12	35.6	17.44	8.050×10^{16}	2.009×10^{-4}	1.700×10^{-5}
5.0	268.41	2.238×10^{0}	3.571×10^{-6}	296.25	35.6	17.41	6.042×10^{16}	2.797×10^{-4}	1.693×10^{-5}
10.0	266.83	1.669×10^{0}	2.679×10^{-6}	295.37	35.6	17.38	4.532×10^{16}	3.728×10^{-4}	1.685×10^{-5}
15.0	265.26	1.244×10^{0}	2.008×10^{-6}	294.50	35.6	17.35	3.398×10^{16}	4.972×10^{-4}	1.677×10^{-5}
20.0	263.69	9.269×10^{-1}	1.505×10^{-6}	293.63	35.6	17.32	2.547×10^{16}	6.635×10^{-4}	1.669×10^{-5}
25.0	262.20	6.901×10^{-1}	1.127×10^{-6}	292.80	35.6	17.26	1.907×10^{16}	8.861×10^{-4}	1.661×10^{-5}
50.0	255.08	1.569×10^{-1}	2.634×10^{-7}	288.80	35.6	17.14	4.457×10^{15}	3.791×10^{-3}	1.625×10^{-5}
75.0	248.11	3.530×10^{-2}	6.091×10^{-8}	284.83	35.6	17.01	1.031×10^{15}	1.639×10^{-2}	1.589×10^{-5}
100.0	241.28	7.848×10^{-3}	1.393×10^{-8}	280.88	35.6	16.87	2.356×10^{14}	7.171×10^{-2}	1.554×10^{-5}
125.0	234.59	1.723×10^{-3}	3.145×10^{-9}	276.95	35.6	16.73	5.322×10^{13}	3.175×10^{-1}	1.518×10^{-5}
150.0	228.02	3.735×10^{-4}	7.013×10^{-10}	273.05	35.6	16.58	1.187×10^{13}	1.424×10^{0}	1.483×10^{-5}
175.0	221.58	7.982×10^{-5}	1.542×10^{-10}	269.17	35.6	16.43	2.610×10^{12}	6.474×10^{0}	1.449×10^{-5}
200.0	216.76	1.696×10^{-5}	3.310×10^{-11}	267.82	35.2	16.24	5.600×10^{11}	2.981×10^{1}	1.437×10^{-5}
300.0	202.30	4.721×10^{-8}	9.103×10^{-14}	269.44	32.4	17.71	1.540×10^{9}	9.996×10^{3}	1.451×10^{-5}
400.0	361.15	8.558×10^{-10}	6.524×10^{-16}	428.55	22.9	31.88	1.104×10^{7}	9.843×10^{5}	2.888×10^{-5}
500.0	626.08	2.334×10^{-10}	7.235×10^{-17}	672.09	16.1	62.55	1.224×10^{6}	6.255×10^{6}	5.018×10^{-5}
600.0	873.46	1.385×10^{-10}	1.874×10^{-17}	1017.29	9.8	82.29	3.171×10^{5}	1.471×10^{7}	7.926×10^{-5}
700.0	952.87	1.090×10^{-10}	1.041×10^{-17}	1210.41	7.6	329.84	1.762×10^{5}	2.040×10^{7}	9.525×10^{-5}
800.0	963.56	8.952×10^{-11}	7.808×10^{-18}	1266.94	7.0	365.80	1.321×10^{5}	2.511×10^{7}	9.991×10^{-5}
900.0	973.60	7.563×10^{-11}	6.017×10^{-18}	1326.59	6.4	402.45	1.018×10^{5}	3.002×10^{7}	1.048×10^{-4}
1000.0	983.06	6.545×10^{-11}	4.744×10^{-18}	1389.83	5.9	439.22	8.026×10^{4}	3.503×10^{7}	1.100×10^{-4}

plained in terms of solar tidal effects. Analysis of the same data by Colombo and Shapiro[24,25] suggests that the rotational period is 58.65 days ($\frac{2}{3}$ of the orbital period) and that the rigidity of the planet is higher than that permitted by Peale and Gold. McGovern, Rasool, and Gross,[26] in their analysis of 50 drawings of Mercury produced from visual observations by Antoniadi, Lyot, and Dollfus, and by Baum, concluded from six pairs of these drawings that, in addition to the previously accepted 88 days, there exist at least three possible values for the rotation rate: 50.1, 58.4, and 70.2 days. Subsequently they indicated[27] that a period of rotation of 43.6 days also could be possible. The best value is believed to be 58.4 ± 0.4 days, since it is consistent with both the radar and observational data. Since the planet has been found not to be in synchronous rotation, the case against an atmosphere becomes somewhat stronger.

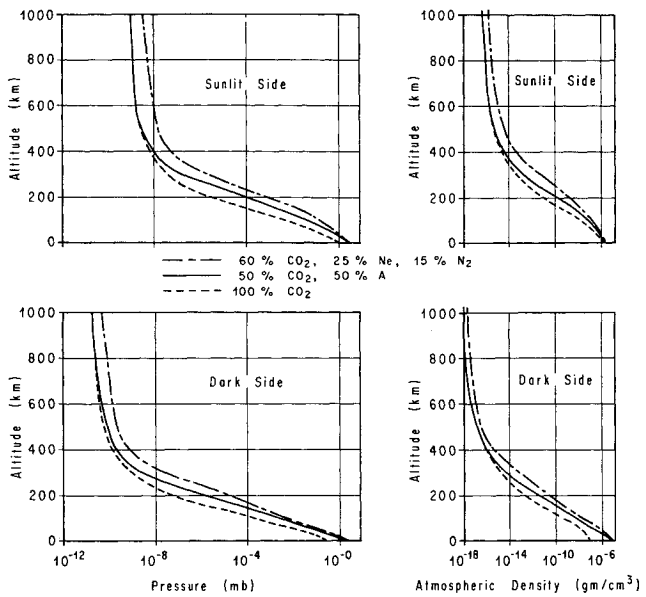

Fig. 1 Atmospheric pressure and density profiles for sunlit and dark-side models of Mercury.

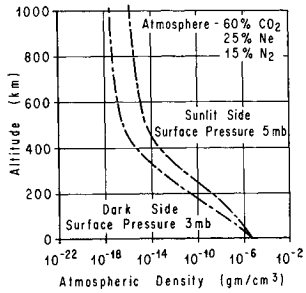

Fig. 2 Typical Mercury atmospheric density operations envelope for maximum density model.

In April 1965, Epstein and his associates,[14,15] in making brightness measurements in the 3.4-mm band, obtained a value of 220° ± 35°K for the dark-side temperature. The most significant finding was that there appeared to be no dependence of temperature on variation in phase. These data seemed to be in disagreement, because other measurements[15] at 8 mm indicated that a large variation with phase should occur at the smaller wavelength of 3 mm if the surface materials of Mercury were like those of the moon. Radio thermal measurements at 1.9 mm by Kraftan-Kassim and Kellermann[28] of the National Radio Astronomy Observatory during February and March 1966 revealed that Mercury's day-to-night range in brightness temperature is ~75°K, centered on a mean value of 288°K. Later, using his 3.4-mm data, Epstein[28] reported that he also found these day-to-night variations. Since the thermal emission originates a few wavelengths below the surface, the temperature a few decimeters below the surface may remain constant at 270°K at least. Since the planet is rotating, the entire surface is being exposed to solar radiation. Therefore, the high dark-side temperature now seems realistic. Since there have been no actual surface temperature measurements for the dark side (antisolar point), the possibility of a meager atmosphere consisting of heavy gases, however, still exists. If a 5-mb atmosphere of CO_2 is present, then atmospheric circulation could be an efficient means of transporting the heat from the day to the night side.

Rasool, Gross, and McGovern[27] have interpreted the spectrographic, polarization, and thermal data to indicate that Mercury has an atmosphere with a probable surface pressure of 0.01 to 10 mb. Using their data as a starting point, several atmospheric models for this planet have been developed by the author to provide the spacecraft design engineer with preliminary environmental criteria for use in spacecraft design studies. In the development of each model, it has been assumed that the atmosphere is not in circulation and that it is stable against gravitational escape and solar wind effects. Figure 1 illustrates profiles of the pressure and density data for the sunlit side and the dark side. Figure 2 illustrates a typical atmospheric density operations envelope for the maximum density model. Tables 2 and 3 present calculated properties (h = geometric altitude, T = kinetic temperature, p = pressure, ρ = density, a = sound speed, $\mathfrak{M}$ = molecular weight, β = density scale height, n = number density, l = mean free path, and μ = viscosity) for each of three atmospheres, for the sunlit and dark sides, respectively. As more data become available, more realistic atmospheric models will be constructed.

References

[1] Weidner, D. K., *A Collection of Papers Related to Planetary Meteorology*, NASA TM X-53693, Jan. 1968, pp. 109–129.

[2] Kuiper, G. P., *The Earth as a Planet*, Vol. 2, The University of Chicago Press, Chicago, 1954.

[3] Kuiper, G. P. and Middlehurst, B. M., *Planets and Satellites*, Vol. 3, The University of Chicago Press, Chicago, 1961.

[4] Kuiper, G. P. and Middlehurst, B. M., *The Moon, Meteorites, and Comets*, Vol. 4, The University of Chicago Press, Chicago, 1963.

[5] Kiess, C. C. and Lassovsky, K., "The Known Physical Characteristics of the Moon and the Planets," TR-11, AD115617, July 1958, Air Research and Development Command, Wright-Patterson Air Force Base, Ohio.

[6] Walker, J. C. C., "The Thermal Budget of the Planet Mercury," *Astrophysical Journal*, Vol. 133, Jan. 1961, pp. 274–280.

[7] Heath, M. B. B., "The Brightness of Mercury at Its Greatest Elongations," *The Journal of the British Astronomical Association*, Vol. 68, 1958, pp. 30–32.

[8] Dollfus, A., "Polarization Studies of Planets," *Planets and Satellites, Solar System II*, edited by G. P. Kuiper and B. M. Middlehurst, The University of Chicago Press, Chicago, 1961.

[9] "News About Mercury (Carbon Dioxide has been Revealed in this Planet's Atmosphere)," TT-65-64151, Oct. 1965, Foreign Technology Div., Wright-Patterson Air Force Base, Ohio.

[10] Spinrad, H. and Hodge, P. W., "An Explanation of Kozyrev's Hydrogen Emission Lines in the Spectrum of Mercury," *Icarus*, Vol. 4, April 1965, pp. 105–108, A65-23491.

[11] Spinrad, H., Field, G. B., and Hodge, P. W., "Spectroscopic Observations of Mercury," *The Astrophysical Journal*, Vol. 141, April 1965, pp. 1155–1160, A65-25226.

[12] Kozyrev, N., "The Atmosphere of Mercury," *The Journal of the British Astronomical Association*, Vol. 73, 1963, pp. 345–346.

[13] Field, G., *The Atmosphere of Mercury*, Wiley, New York, 1964, pp. 269–276.

[14] Epstein, E. E., "Disk Temperatures of Mercury and Mars at 3.4 mm," *The Astrophysical Journal*, Vol. 143, Feb. 1966, pp. 597–598.

[15] Epstein, E. E., Oliver, J. P., and Schorn, R. A., "Further Observations of Planets and Quasi-Stellar Radio Sources at 3 mm," TR-669 (9230-04)-1, SSD TR-66-122, Ad-487-702, Contract AF 04(695)-669, NAS7-100, July 1966, Laboratory Operation, Aerospace Corp., El Segundo, Calif.

[16] Kozyrev, N. A., "The Atmosphere of Mercury," *Sky and Telescope*, Vol. 27, 1964, pp. 338–341.

[17] Sandner, W., *The Planet Mercury*, Faber and Faber, London, 1963.

[18] Howard, W. E., Barrett, A. H., and Haddock, F. T., "Measurement of Microwave Radiation from the Planet Mercury," *The Astrophysical Journal*, Vol. 136, 1962, pp. 995–1004.

[19] Barrett, A. H., "Passive Radio Observations of Mercury, Venus, Mars, Saturn, and Uranus," *Journal of Research, Sec. D—Radio Science*, Vol. 69D, Dec. 1965.

[20] Welch, W. J. and Thornton, D. D., "Recent Planetary Observations of Wavelengths Near 1 cm," *The Astronomical Journal*, Vol. 70, No. 2, 1965, pp. 149–150.

[21] Pettengill, G. H. and Dyce, R. B., "A Radar Determination of the Rotation of the Planet Mercury," *Nature*, Vol. 206, No. 4990, June 1965, p. 1240.

[22] Pettengill, G. H., "Recent Arecibo Observations of Mercury,"

Journal of Research, Sec. D—Radio Science, Vol. 69D, Dec. 1965, pp. 1627–1628.

[23] Peale, S. J. and Gold, T., "Rotation of the Planet Mercury," *Nature,* Vol. 206, No. 4990, June 1965, pp. 1240–1241.

[24] Colombo, G., "Rotational Period of Mercury," *Nature,* Nov. 1965, pp. 575.

[25] Colombo, G. and Shapiro, I., "The Rotation of the Planet Mercury," *The Astrophysical Journal,* Vol. 145, July 1966.

[26] McGovern, W. E., Gross, S. H., and Rasool, S. I., "Rotation Period of the Planet Mercury," *Nature,* Vol. 208, Oct. 1965, p. 375.

[27] Rasool, S. I., Gross, S. H., and McGovern, W. E., "The Atmosphere of Mercury," TM X-57322, 1966, NASA.

[28] Kaftan-Kassim, M. A. and Kellermann, K. I., "Temperature of Mercury," *Sky and Telescope,* Vol. 30, April 1967.

[29] Krause, H. G., "Astronomical Constants of the Solar System," unpublished manuscript, 1965, NASA Marshall Space Flight Center, Huntsville, Ala.

[30] Ray, A. E., *Foundations of Astrodynamics,* Macmillan, New York, 1965.

[31] de Vaucouleurs, G., "Geometric and Photometric Parameters of the Terrestrial Planets," *Icarus,* Vol. 3, 1964, pp. 187–235.

[32] Brandt, J. C. and Hodge, P. W., *Solar System Astrophysics,* McGraw-Hill, New York, 1964, p. 367.

A Method for Comparing Ballistic and Electric Propulsion Performance

Federico G. Casal*
NASA Mission Analysis Division, Moffett Field, Calif.

Nomenclature

B = area of ballistic superiority
b,e,f = cost coefficients
C = boundary of equal cost
H = area of hybrid superiority
M_B = Earth orbital mass of ballistic system
M_H = Earth orbital mass of hybrid system
M_W = mass of propulsive powerplant
n = scaling exponent
P = power level
τ = minimum energy flight time

Introduction

THREE primary benefits are attributed to the use of nuclear-electric upper stages: reduction of trip time to the outer planets, increase in payload capacity beyond low Earth orbit, or reduction of launch vehicle requirements for a given payload.[1] To what extent one or more of these potential benefits may be realized depends on the applied groundrules, on powerplant specific mass, and on cost considerations.[2]

This Note describes a method which permits systematic exploration of the effects of the groundrules, the uncertainties in the performance parameters, and the major cost tradeoff factors which will later influence economic comparisons between space propulsion systems exhibiting widely differing characteristics. The two different systems singled out for treatment in this paper are the "ballistic" (consisting of high-thrust stages only) and the "hybrid" (consisting of combination of high-thrust and nuclear-electric stages).

Method

The general approach begins with specification of the target and the gross magnitude of the payload. Mission groundrules include capture orbit characteristics and allowable trip time. The trajectory problem and the systems optimization problem are solved in iterative fashion for both the hybrid and the ballistic case. For the examples presented in this particular Note, this has been accomplished by the use of a very fast numerical code.[3] The points at which the hybrid and the ballistic systems produce the same results constitute boundaries of equal performance. Some consideration will also be given to certain cost tradeoff functions.

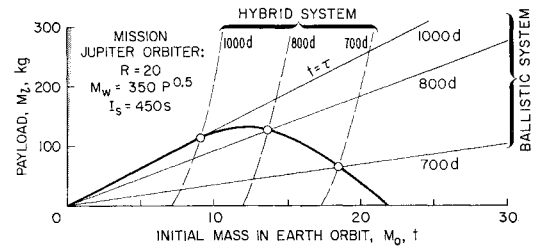

Fig. 1 Boundary of equal performance between hybrid and ballistic systems.

For planetary missions, the characteristics of the capture orbit strongly influence the propulsive requirements; and since the trip time/payload characteristics of high-thrust and low-thrust systems are radically different, the capture orbit and trip time groundrules can strongly influence the outcome of the comparison. Ballistic systems generally exhibit a trend in which the inert mass fraction decreases with increasing mass of the stage but increases with increasing specific impulse. For the sake of simplicity, only a specific impulse of 450 sec and a constant stage inert mass fraction of 10% of the propellant mass is considered in this paper. For nuclear-electric powerplants, the total mass grows with the power level of the entire system. An expression fitting a wide variety of powerplant designs[4–7] is

$$M_w = 350P^n \tag{1}$$

in which M_W is the mass of the powerplant in kilograms, P is the power level in kilowatts, and the exponent n is equal to 0.6 for the "conservative," 0.5 for the "nominal," and 0.4 for the "advanced" technology estimates. To simplify the comparisons presented in this paper, $n = 0.5$ will generally be used. It is assumed that both the hybrid and the ballistic system utilize a chemical cryogenic Earth escape stage. In the hybrid cases, this stage is used to obtain optimum hyperbolic excess velocity before operation of the electrical stage. For the ballistic cases, capture is obtained by means of a high-thrust rocket with a specific impulse of 300 sec. In the hybrid case and for the capture orbits considered in this paper (circular orbits around the most massive planets), the electrical capture mode yields more payload.

The general capabilities of ballistic and hybrid systems are shown in Fig. 1. The specific mission considered is a Jupiter orbiter with a circular capture orbit at an altitude of 20 planetary radii. Both systems are of continuously variable size. The nuclear electric powerplant follows the scaling law of Eq. (1). The initial mass in Earth orbit (M_0) is used merely to typify vehicle size and by no means implies a necessity to depart from Earth orbit. The straight thin lines represent the capability of the ballistic system for three constant trip times whereas the broken lines represent the capabilities of the hybrid system for the same three trip times. A trip time of 1000 days approximately corresponds to the minimum energy requirement and, therefore, yields maximum payload for the ballistic system in the simple two-impulse mode. For a trip time of roughly 600 days, the ballistic payload vanishes entirely.

At any specific trip time, the ballistic and the hybrid capability lines intersect at the point where both systems can carry the same payload for the same size of launch vehicle in the same trip time. These points of equal performance

Presented as Paper 69-249 at the AIAA 7th Electric Propulsion Conference, Williamsburg, Va., March 3–5, 1969; submitted March 10, 1969; revision received August 4, 1969.

* Assistant Director for Propulsion Systems. Member AIAA.